Available online at www.sciencedirect.com
SCIENCE DIRECT®
Optical Fiber Technology 10 (2004) 91–123
Optical Fiber Technology
www.elsevier.com/locate/yofte

Transient gain dynamics in saturated Raman amplifiers

A. Bononi,* M. Papararo, and M. Fuochi

Dipartimento di Ingegneria dell'Informazione, Università di Parma, Parma, Italy

Received 14 May 2003; revised 28 August 2003

Abstract

This paper provides a detailed analysis of transient gain dynamics in saturated Raman amplifiers fed by wavelength division multiplexed (WDM) signals. Such dynamics are due to a pump saturation effect, known as pump-mediated signal-to-signal crosstalk, which is equivalent to the well-known cross-gain modulation in EDFAs. We provide for the first time a simple block-diagram model of the Raman amplifier, whose *state* is represented by the *relative pumps depletion* sensed by the signals. With such model, we are able to prove that the time constants of the Raman gain transients are of the same order as the pump–signal walk-off times. For counter-propagating pumps, the model is very accurate in predicting both the steady-state gain and the transient gain dynamics, with more than an order of magnitude improvement in computation time with respect to the direct solution of the signals and pumps propagation equations. The value of such model is therefore in the simulation of dynamic WDM networking scenarios in which the input powers have large swings in time. The model also extends to the co-propagating pump and well captures the time constants involved in the transients, although the accuracy in the predicted power levels is worse than that of the counter-propagating pump case.

1. Introduction

Transient gain dynamics in saturated doped-fiber amplifiers have been studied intensively in connection with sudden channel addition or removal in wavelength division multiplexed (WDM) systems caused by either unintentional failures, or by deliberate network reconfigurations [1,2]. The main concern is the duration of the power transients, which may induce temporary performance degradation, and the amount of power surges,

* Corresponding author.
E-mail address: alberto@tlc.unipr.it (A. Bononi).

1068-5200/$ – see front matter
doi:10.1016/j.yofte.2003.09.002

which may damage the optical components and cause system disruption. Such transients are connected to the population dynamics of the dopant ions, and can be much faster than the ions relaxation time, depending on the signals saturating power [2–4].

Surprisingly, such gain transients have recently been experimentally observed even in counter-pumped single-channel saturated Raman amplifiers [5], although no ions are involved in the amplification process. The reason is that the strong power of the signal leading edge depletes the injected pump, and thus the main body of the signal pulse does not enjoy the same high gain as the signal front. Such transients can be numerically reproduced by solving the coupled time-dependent propagation equations for signals and pumps, and are connected to the signal–pump walk-off [5]. Simulation and experimental results with two WDM channels and multiple counter-propagating pumps were also reported in [6].

In this paper, we first show that the gain dynamics in the single counter-pumped Raman amplifier can be accurately predicted by determining the time behavior of a single state variable, namely, the relative pump change sensed by the signals. Such state-variable model provides dramatic savings in transients computation times with respect to the complete propagation model, larger savings being connected to larger WDM channels count. The state model is similar to the state model for erbium doped fiber amplifiers (EDFA) [4], and is thus amenable to a simple block-diagram implementation, which makes it attractive for block-oriented optical network simulators [7]. Next, we extend the model to the case of multiple counter-propagating pumps, and we show that it accurately predicts the dynamics of practical wide-band Raman amplifiers. Since the multi-pump model makes a fundamental distinction between signals and pumps, when such distinction gets blurred, such as in resonant pumping, the accuracy of the model is reduced, and we quantify such reduction.

It is known that transient gain dynamics are present also in co-pumped Raman amplifiers, with transients occurring on a much faster time scale than in counter-pumped amplifiers [6,8]. We develop here a state-variable model also for the co-pumped case, which we use to predict the time constants of the transients. However, our model strongly relies on the peculiar feature that the pump-saturating signal power abruptly increases towards the amplifier output, which is true for most counter-pumped amplifiers, and is only an approximation for co-pumped amplifiers. Hence the model is less accurate for co-pumped amplifiers, although the time constants are correctly reproduced.[1]

This paper is organized as follows. In Section 2 we introduce the propagation equations, and provide their formal implicit solution under specified simplifying assumptions. In Section 3 we derive the model for the single counter-propagating pump case. In Section 4 we test the accuracy of the model with respect to the exact solution, and explore several examples of gain dynamics. We then study the steady-state equation and provide a linearization of the model in order to obtain explicit expressions for the time constants involved in the transients. In Section 5 we explain how to include pump relative intensity noise into the model. Section 6 deals with the extension of the model to the multiple pump case, while Section 7 provides its numerical validation. Finally, Section 8 tackles the co-propagating pump case.

[1] Some discrete Raman amplifiers use a combination of different fibers to achieve a more complex gain-length profile even in the counter-pumped configuration. The accuracy in such case might be reduced as well.

2. Propagation equations

Assume N WDM signals, at wavelengths λ_j, $j = 1, \ldots, N$, propagate along a fiber at the same group velocity υ_s, and a single pump at a shorter wavelength λ_p propagates at velocity υ_p.

By casting the propagation equations [9] in the signals and pump *retarded time frames* $t_s \triangleq t - z/\upsilon_s$ and $t_p \triangleq t - z/\upsilon_p$, one gets

$$\begin{aligned}
&\frac{\partial}{\partial z} P(t_p, z) = \pm \left[\alpha_p + \sum_{j=1}^{N} \hat{c}_{jp} S_j(t_p - dz, z) \right] P(t_p, z), \\
&\frac{\partial}{\partial z} S_j(t_s, z) = \left[-\alpha_j + c_{jp} P(t_s + dz, z) + \sum_{i=1}^{N} c_{ji} S_i(t_s, z) \right] S_j(t_s, z), \\
&\quad j = 1, \ldots, N,
\end{aligned} \tag{1}$$

where $P(t, z)$ and $S_j(t, z)$ are the pump and signal powers [W] at time t and coordinate z; α_p and α_j is the attenuation of pump and signals, respectively; $d \triangleq (1/\upsilon_s - 1/\upsilon_p)$ is the walk-off parameter; the coefficient $c_{ji} \triangleq \gamma_{ji}$ if $\lambda_j > \lambda_i$ and $c_{ji} \triangleq -\gamma_{ji}\lambda_i/\lambda_j$ if $\lambda_j < \lambda_i$, where $\gamma_{ji} = \gamma_{ij} > 0$ is the Raman gain efficiency coefficient [$\mathrm{W}^{-1}\,\mathrm{km}^{-1}$] between wavelengths λ_i and λ_j; and finally $\hat{c}_{jp} \triangleq -c_{pj}$, which is a positive quantity for all signals j.

The top sign in the $\pm$ symbol in the first equation refers to the counter-propagating pump, for which $\upsilon_p < 0$, while the lower sign to the co-propagating pump, for which $\upsilon_p > 0$. In the above equations we neglected spontaneous Raman scattering, and Rayleigh backscattering. The summation term in the signal propagation equation accounts for the direct signal to signal Raman crosstalk.

The formal solution of (1) can be obtained by separating the variables and integrating from the input coordinate (z_{is} for signals and z_{ip} for pump) to the output coordinate (z_{os} for signals and z_{op} for pump) as

$$\begin{cases}
P(t_p, z_{\mathrm{op}}) = P(t_p, z_{\mathrm{ip}}) \exp\Big\{ \pm \Big[\alpha_p (z_{\mathrm{op}} - z_{\mathrm{ip}}) \\
\qquad\qquad + \sum_{j=1}^{N} \hat{c}_{jp} \int_{z_{\mathrm{ip}}}^{z_{\mathrm{op}}} S_j(t_p - d\,z, z)\, dz \Big] \Big\}, \\
S(t_s, z_{\mathrm{os}}) = S(t_s, z_{\mathrm{is}}) \exp\Big\{ -\alpha_j (z_{\mathrm{os}} - z_{\mathrm{is}}) + c_{jp} \int_{z_{\mathrm{is}}}^{z_{\mathrm{os}}} P(t_s + dz, z)\, dz \\
\qquad\qquad + \sum_{i=1}^{N} c_{ji} \int_{z_{\mathrm{is}}}^{z_{\mathrm{os}}} S_i(t_s, z)\, dz \Big\}.
\end{cases} \tag{2}$$

To make the analysis tractable, in the following we will neglect the direct signal-to-signal Raman crosstalk in the Raman amplifier. While in most discrete Raman amplifiers such crosstalk is negligible, since the signal powers rise to large values only close to the output, in distributed Raman amplifiers most direct signal-to-signal Raman crosstalk occurs in the first kilometers of the transmission fiber, where no amplification is present. Hence such crosstalk can be easily accounted for analytically using well known methods [10], and then the modified input can be used in our simplified model.

3. Counter-propagating pump

In this case the pump is injected at $z_{\rm ip} = L$, and the signals enter at $z_{\rm is} = 0$, where L is the fiber length, and we assume that $\upsilon_p = -\upsilon_s$, so that $d = 2/\upsilon_s$. From (2), the solution of the simplified propagation equations for the counter-propagating pump case at coordinate $z_{\rm op} = z_{\rm os} = z \leqslant L$ is

$$\begin{cases} S_j(t_s, z) = S_j^{\rm in}(t_s) \exp\{-\alpha_j z + c_{jp} \int_0^z P(t_s + dz', z')\, dz'\}, \\ P(t_p, z) = P_0 e^{-\alpha_p (L-z)} e^{-\Gamma(t_p, z)}, \end{cases} \tag{3}$$

where $P_0 \triangleq P(t_p, L)$ is the constant injected pump power, $S_j^{\rm in}(t_s) \triangleq S_j(t_s, 0)$ is the input signal waveform, and

$$\Gamma(t_p, z) \triangleq \sum_{j=1}^{N} \hat{c}_{jp} \int_z^L S_j(t_p - dz', z')\, dz' \tag{4}$$

is a quantity defined in the pump retarded frame. For moderate pump depletion, i.e., $\Gamma < 0.3$, we can approximate

$$e^{-\Gamma} \cong 1 - \Gamma, \tag{5}$$

with an error below 5% (i.e., below 0.2 dB), so that from the second of (3) we get $P(t_p, z) \cong \overline{P}(z)(1 - \Gamma(t_p, z))$, where $\overline{P}(z) \triangleq P_0 e^{-\alpha_p (L-z)}$ is the undepleted pump profile, and thus

$$\Gamma(t_p, z) \cong \frac{\Delta \overline{P}(t_p, z)}{\overline{P}(z)}, \tag{6}$$

where $\Delta \overline{P}(t_p, z) \triangleq \overline{P}(z) - P(t_p, z)$, so that we *physically interpret Γ as the relative pump variation caused by saturation, measured in the pump retarded time frame at coordinate z.*

Using the *key approximation* (5), the integral term in the signal equation in (3) becomes

$$c_{jp} \int_0^z P(t_s + dz', z')\, dz' = g_j(z)\big(1 - x(t_s, z)\big), \tag{7}$$

where we defined

$$\begin{cases} g_j(z) \triangleq (e^{-\alpha_p L}(e^{\alpha_p z} - 1)) \frac{c_{jp} P_0}{\alpha_p}, \\ x(t_s, z) \triangleq \frac{c_{jp} P_0}{g_j(z)} \int_0^z e^{-\alpha_p (L - z')} \Gamma(t_s + dz', z')\, dz'. \end{cases} \tag{8}$$

The first row defines the undepleted on-off *logarithmic gain* $g_j(z)$, while the undepleted gain vs z profile is [11]

$$G_j(z) = \exp\big(-\alpha_j z + g_j(z)\big). \tag{9}$$

The second definition in (8) can be interpreted as follows. Once (7) is plugged in (3) we get the signal power at z as

$$S_j(t_s, z) = S_j^{\rm in}(t_s) \exp\big\{-\alpha_j z + g_j(z)\big(1 - x(t_s, z)\big)\big\}, \tag{10}$$

and since the term $(1 - x(t_s, z))$ multiplies the injected pump P_0 hidden in $g_j(z)$, we see that $x(t_s, z)$ *physically represents the relative pump depletion sensed by the signal in its retarded time frame at coordinate* z.

Now let $x(t_s) \triangleq x(t_s, L)$ be the depletion at the output, and $g_j \triangleq g_j(L)$, so that the output signals can be written as

$$S_j^{\text{out}}(t_s) \triangleq S_j(t_s, L) = S_j^{\text{in}}(t_s) \exp\{-\alpha_j L + g_j(1 - x(t_s))\}, \tag{11}$$

and from (8) one can write

$$x(t_s) = \frac{1}{L_p} \int_0^L e^{-\alpha_p(L-z)} \Gamma(t_s + dz, z)\, dz, \tag{12}$$

being

$$\frac{g_j}{c_{jp} P_0} = \frac{1}{P_0} \int_0^L \overline{P}(z)\, dz = (1 - e^{-\alpha_p L})/\alpha_p \triangleq L_p$$

the effective fiber length at λ_p. Using (6) in (12) we also get another physical interpretation of x,

$$x(t_s) = \frac{\int_0^L \Delta \overline{P}(t_s + dz, z)\, dz}{\int_0^L \overline{P}(z)\, dz}, \tag{13}$$

which clarifies by comparison with (6) the similarity between x and Γ: x *is the relative integrated pump variation, measured in the signals retarded time frame*.

We now use (12) to determine the time evolution of $x(t_s)$. Once $x(t_s)$ is known, the time evolution of all the output signals is immediately obtained through (11). We use (10) in (4), and plug the result in (12) to get

$$x(t_s) = \frac{1}{L_p} \sum_{j=1}^{N} \hat{c}_{jp} \int_0^L e^{-\alpha_p(L-z_1)} \left\{ \int_{z_1}^L S_j^{\text{in}}(t_s + d(z_1 - z_2)) \times G_j(z_2) \exp\left[-g_j(z_2) x(t_s + d(z_1 - z_2), z_2)\right] dz_2 \right\} dz_1. \tag{14}$$

Such equation is quite complex, but it can be drastically simplified by recalling that the $G_j(z)$ profile very sharply arises in the last few meters of the Raman amplifier, so that we can use the term $G_j(z_2) \exp[-g_j x(t_s + d(z_1 - z_2), L)]$ instead of the exact saturated gain $G_j(z_2) \exp[-g_j(z_2) x(t_s + d(z_1 - z_2), z_2)]$ in the above integral:

$$x(t_s) \cong \frac{1}{L_p} \sum_{j=1}^{N} \hat{c}_{jp} \int_0^L e^{-\alpha_p(L-z_1)} \left\{ \int_{z_1}^L S_j^{\text{in}}(t_s - d(z_2 - z_1)) \times \exp\left[-g_j x(t_s - d(z_2 - z_1))\right] G_j(z_2)\, dz_2 \right\} dz_1. \tag{15}$$

What we gain is that now we have an integral equation in the only unknown $x(t_s)$. We solve it by making the following change of integration variables: $\tau = d(z_2 - z_1)$; $z' = z_1$. After the change, by dividing and multiplying by $G_j(L)$, one finally gets

$$x(t_s) = \sum_{j=1}^{N} \int_0^{dL} S_j^{\text{in}}(t_s - \tau) e^{[-\alpha_j L + g_j[1 - x(t_s - \tau)]]} \times \frac{\hat{c}_{jp}}{dL_p G_j(L)} \left(\int_0^{L-\tau/d} e^{-\alpha_p(L-z')} G_j(z' + \tau/d)\, dz' \right) d\tau,$$

where the integration is easily recognized as a convolution operation. Hence, the state variable $x(t_s)$ approximately satisfies the following implicit integral equation

$$x(t_s) = \sum_{j=1}^{N} S_j^{\text{out}}\big(t_s, x(t_s)\big) \otimes h_j(t_s), \tag{16}$$

where $S_j^{\text{out}}(t_s, x(t_s))$ is given in (11), the symbol $\otimes$ denotes convolution, and h_j is the impulse response of a linear filter:

$$h_j(t) = \frac{\hat{c}_{jp}}{dL_p G_j(L)} \left[\int_0^{L-t/d} e^{-\alpha_p(L-z')} G_j\left(z' + \frac{t}{d}\right) dz' \right] \Pi\left(\frac{t - dL/2}{dL}\right), \tag{17}$$

where $G_j(z)$ is the undepleted gain-versus-z profile (9), and $\Pi(x) = 1$ for $-0.5 < x < 0.5$ and zero else. In Appendix A, a closed form of the impulse response (17) is provided, along with its exponential approximation for distributed Raman amplifiers (A.3).

The fundamental equation (16) can be solved recursively, by performing the numerical convolution on the right hand side, and updating $x(t_s)$ as the average between its old value and its new value obtained from the convolution, in order to smooth out the (possibly) large fluctuations from one convolution to the next. Convergence to the final solution is usually obtained within some tens of iterations, a number that increases with the amount of amplifier saturation.

3.1. Numerical verifications

We tested the accuracy of our state-variable model against the exact solution of the propagation equations, starting from the experimental setup used in [5]. The input signal was a single-wavelength sequence of two contiguous packets of duration 400 μs each, the first with power 1 mW and the second 0.1 mW, entering $L = 14$ km of dispersion compensating fiber (DCF) at time $t = 0$.[2] In the model, we used $\alpha_j = 0.46$ dB/km, $\alpha_p = 0.6$ dB/km, $c_{jp} = 2$ [W^{-1} km^{-1}], corresponding to a dispersion compensating fiber (DCF) with signal wavelength $\lambda_j = 1545.3$ nm, and pump wavelength $\lambda_p = 1454.7$ nm [5].

[2] Another interpretation of the same input sequence may be the following: at time $t = 0$, 10 channels (on very closely spaced wavelengths) having 0.1 mW power each are fed to an initially unsaturated Raman amplifier, while at time 400 μs nine out of ten channels are dropped.

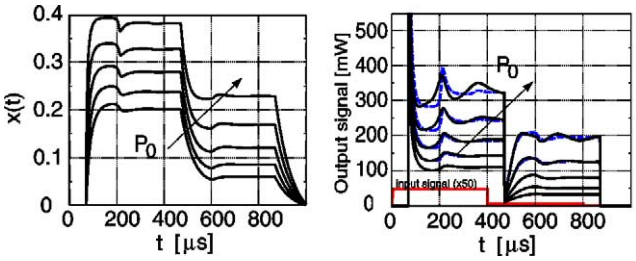

Fig. 1. (Left) Relative pump change sensed by the signal, and (right) output signal power, for increasing levels of pump power $P_0 = 0.64, 0.70, 0.77, 0.86, 0.97$ W. Solid lines: exact solution (1); dashed lines: model (16). Input signal shown (right) magnified 50 times.

Figure 1 shows the relative pump change $x(t)$ (left) and the output signal power $S_j^{\text{out}}(t)$ (right) in the absolute time frame $t = t_s(0)$, calculated as in (16), (11) (dashed lines), and the exact numerical solution of the propagation equations (1) (solid lines). Five different curves are reported in each sub-figure, obtained for pump powers $P_0 = 0.64, 0.70, 0.77, 0.86, 0.97$ W, corresponding to saturated gains of 20 to 24 dB, respectively.[3]

In the figure, we first note that the effect of deep saturation is to alter the steady-state power ratio between the first and the second pulse, starting from $1/10$ in the linear regime, down to $2/3$ at $P_0 = 0.97$ W. We next note that the approximate solution (16) very well reproduces the exact numerical solution as long as $x < 0.3$, the approximation becoming worse when the linearization $e^{-\Gamma} \cong 1 - \Gamma$ fails, i.e., $\Gamma > 0.3$. An analytical explanation of this fact will be postponed to Section 4, Eq. (26). The time constants of the transients are somewhat faster than (but comparable to) the walk-off time $dL = 140$ μs, while the propagation delay within the amplifier is $L/\upsilon_s = 70$ μs, where $\upsilon_s = 2 \times 10^8$ m/s. A thorough discussion of the time constants is postponed to Section 5. One notable difference with transients in EDFAs is the presence of ringing in the step response even in a single Raman amplifier. Such ringing disappears at small pump powers, and will be further discussed in Section 5.

As stated in the Introduction, one concern in the transients are the power surges that may damage the optical components. As seen in the figure, the power spike at the signal leading edge can be many times the steady-state saturated value reached after the transient, and can be quantified through the *power sag* across the pulse, which we define as

$$\text{SAG} \triangleq \frac{S_j^{\text{out}}(x=0)}{S_j^{\text{out}}(x^{\text{ss}})} = e^{g_j x^{\text{ss}}},$$

where ss denotes the steady state values reached after the transient, and we used (11). Hence the sag across the pulse becomes larger for increasing undepleted on/off gain e^{g_j},

[3] At such very large signal powers propagating inside the Raman amplifier, Brillouin scattering, which we do not include in our equations, is known to deeply affect propagation [17]. However, the reason of using such very large pump and saturated gain values is to test up to which level of pump depletion x the accuracy of the model (16) versus the exact solution of (1) is acceptable.

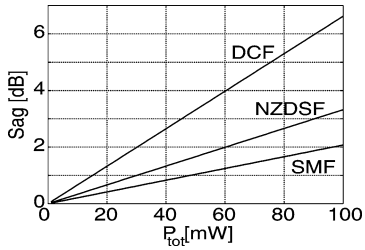

Fig. 2. Pulse sag (19) versus total output signal power $P_{\text{tot}} = \sum_i S_i^{\text{out}}(x^{\text{ss}})$ for various types of fiber, DCF, NZDSF, SMF, having respectively Raman gain $c_{jp} = [2.0, 0.46, 0.31]$ [$\text{W}^{-1}\,\text{km}^{-1}$], $\lambda_j = 1545.3$ nm, $\lambda_p = 1454.7$ nm, and pump attenuation $[0.60, 0.28, 0.30]$ dB/km.

i.e., for increasing pump P_0, but also for increasing stead-state saturation

$$x^{\text{ss}} = c \cdot \frac{\sum_i S_i^{\text{out}}}{P_0}, \tag{18}$$

where we have *conjectured* that such steady state saturation increases linearly with the total signal power relative to the pump, a relation that will be shown to approximately hold in the next section, where it will be shown that $c \cong \lambda_j/\lambda_p$, being λ_j the average signal wavelength. Hence from (8) and (18) we see that the pump power P_0 cancels out in the exponent, so that the sag in dB is

$$\text{SAG}_{\text{dB}} \cong (10\log_{10} e)\frac{c_{jp}}{\alpha_p}\frac{\lambda_j}{\lambda_p}\sum_i S_i^{\text{out}}(x^{\text{ss}}) \tag{19}$$

from which we conclude that the power sag on a pulse depends on (i) the *total output signal power*; and (ii) on the *fiber type* through its Raman gain, and its pump loss. Figure 2 shows the power sag (19) versus total output signal power $P_{\text{tot}} = \sum_i S_i^{\text{out}}(x^{\text{ss}})$ for various fiber types. We note that for the DCF in our example, the sag exceeds 3 dB (large saturation effects) when the output signal power exceeds 50 mW, while it remains below 1 dB (negligible saturation effects) when the signal power is below 10 mW. A power larger than 100 mW is required to significantly saturate a Raman amplifier that uses SMF fiber.

The Raman saturated case is very similar to the case of saturated EDFAs. Starting from Eq. (6) in [4], one can prove that the power sag across a pulse in an EDFA is given by

$$\text{SAG}_{\text{dB}} \cong (10\log_{10} e)B_j\tau\sum_i\left(S_i^{\text{out}}(x^{\text{ss}}) - S_i^{\text{in}}\right), \tag{20}$$

where the parameter B_j and the fluorescence time τ are defined in [4], and their product is proportional to the inverse of the intrinsic saturation power $S_j^{\text{is}} = h\nu_j/B_j\tau$ [W] by the photon energy $h\nu_j$. Therefore by similarity with such result, one may define for the saturated Raman amplifier the *intrinsic saturation power at* λ_j as

$$S_j^{\text{is}} \triangleq \frac{\lambda_p}{\lambda_j}\frac{\alpha_p}{c_{jp}}, \tag{21}$$

and thus the previous result can be reworded by saying that the sag exceeds 3 dB when the total output power exceeds $3/(10\log_{10} e) \cong 0.7$ times the intrinsic saturation power.

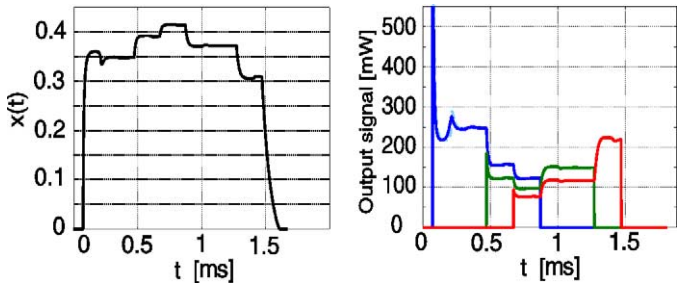

Fig. 3. Example 2. (Left) Relative pump change sensed by the signal, and (right) output signals power, for pump power $P_0 = 0.86$ W. Solid lines: exact solution (1); dashed lines: model (16).

We next provide a second example in which several WDM signals are fed to the same discrete amplifier previously described. The input signals we used were three channels at wavelengths [1552.2, 1552.6, 1553.0] nm, each carrying a single packet of duration 800 μs and power 1 mW. The packet on channel 1 entered the amplifier at time $t = 0$, the one on channel 2 entered at $t = 400$ μs, and the one on channel 3 at $t = 600$ μs. The injected pump power was $P_0 = 0.86$ W, with signal Raman gains $c_{jp} = [2.1, 2.0, 2.0]$ W^{-1} km^{-1}. Figure 3 (left) shows the relative pump change $x(t)$ and (right) the output signals power, the exact solution (1) being in solid line, and the model (16) in dashed line. Again, the reason why we used such large pump powers is to test the accuracy and the range of applicability of the model. We note that the analytical solution very well matches with the exact one. We can clearly see the effect of the pump-mediated signal to signal crosstalk, the largest saturation occurring when all three packets are simultaneously present in the amplifier. Note that the effect of one packet lasts for about one walk-off time dL after its end. Hence the "memory" of the system, i.e., its *gain recovery time*, is slightly less than the walk-off time in this example, and never exceeds dL. Such walk-off time plays in Raman amplifiers the same role as the fluorescence time plays in EDFAs. This will be evident after the discussion in Section 5.

Having established that the model well matches the simulations, we now wish to present more results of single-pump single-channel transients, in order to check similarities and differences with the transients observed in EDFAs [4]. The discrete amplifier for the next examples consisted of $L = 10$ km of DCF, with peak Raman gain coefficient $c_{\max} = 3.2$ W^{-1} km^{-1}, Pump wavelength $\lambda_p = 1450$ nm, and signal wavelength $\lambda_s = 1550$ nm, with 1 mW peak input signal power.

We first illustrate the amplifier dynamics in a packet switching scenario. We started by examining the case of one input signal packet of duration 400 μs, which is much longer than the time response of the filter $h_j(t)$ in Eq. (11). In Fig. 4, dashed lines show the dynamics of the relative pump depletion $x(t)$, and of the amplified signal $S_j^{\text{out}}(t)$ when the input pump power has a *moderate* value of pump $P_0 = 200$ mW. We note exponential-like transients which last around 100 μs, which are quite similar in nature to those observed in EDFAs [4]. We will show in Section 5 a simple formula for the transient time constants in this *moderate pump* case.

If the pump power is increased to a *large* value $P_p = 400$ mW, we note in Fig. 5, dashed lines, that the time behavior of $x(t)$ and $S_j^{\text{out}}(t)$ starts to show a resonance overshoot,

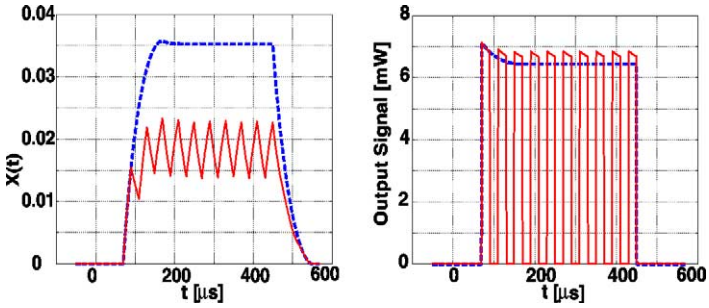

Fig. 4. Time evolution of (left) relative pump depletion, and (right) output signal, in response to (dashed) a single packet of duration 400 μs; (solid) a train of pulses of duration $T_p = 20$ μs and pulse separation $T_r = T_p$. Input pump power $P_0 = 200$ mW.

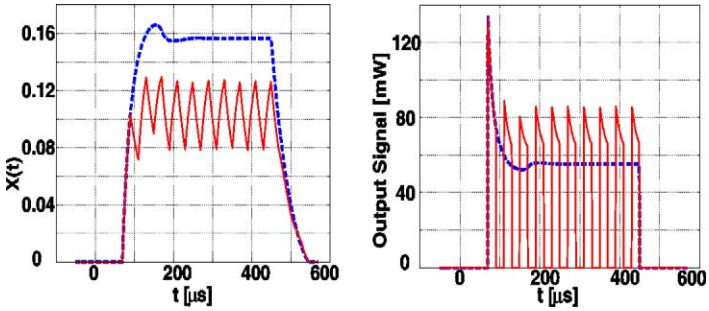

Fig. 5. Time evolution of (left) relative pump depletion, and (right) output signal, in response to (dashed) a single packet of duration 400 μs; (solid) a train of pulses of duration $T_p = 20$ μs and pulse separation $T_r = T_p$. Input pump power $P_0 = 400$ mW.

which is not present in transients involving EDFAs [4]. Moreover, a larger pump implies larger signal-induced gain saturation, which justifies a larger power sag across the output packet. We already saw in Eq. (19) that the power sag across a pulse is directly proportional to the total signal power, which linearly increases with pump power. Such behavior is different from saturation in EDFAs, Eq. (20), where the power sag is still proportional to the total output signal power, but such power *saturates* for increasing pump power, since the population inversion cannot exceed a maximum value x^{ss} smaller than one [4].

Next, we examined the response of the amplifier to an input train of equally spaced pulses of fixed duration $T_p = 20$ μs, a time much shorter than the time response of the filter $h_j(t)$. The results are displayed in Figs. 4–6 in solid lines.

In Fig. 4 the gap between pulses is $T_r = T_p$ and the input pump power is $P_0 = 200$ mW. We note that the response to the first packet obviously coincides with the dashed-line curve, while the response to the following packets exceeds the dashed line, since the pump refills in the lull between packets, with a time constant that we can infer from the upward transition of the dashed-line curve of $x(t)$. Physically, such pump refill is due to fresh back-propagating pump photons reaching the traveling signal pulse.

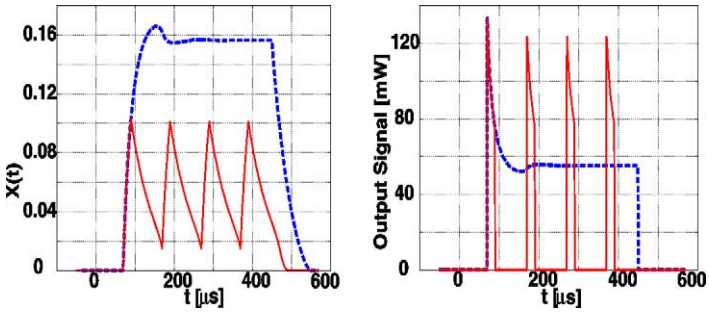

Fig. 6. Time evolution of (left) relative pump depletion, and (right) output signal, in response to (dashed) a single packet of duration 400 μs; (solid) a train of pulses of duration $T_p = 20$ μs and pulse separation $T_r = 3T_p$. Input pump power $P_0 = 400$ mW.

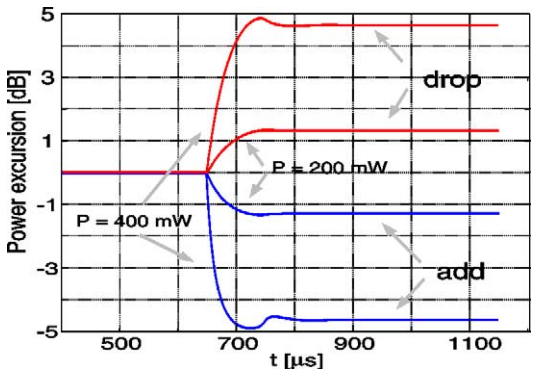

Fig. 7. Output power excursion for the surviving channel $\lambda = 1552.4$ when adding or dropping 7 out of 8 channels.

If the pump value is increased to 400 mW, as seen in Fig. 5, both the pump depletion and refill processes become faster, so that we see a faster power sag across the pulses, as well as a larger peak power on the pulses following the first one. In any case, we note that the locus of the peaks follows the power profile of the dashed line.

In Fig. 6 we kept $P_0 = 400$ mW, and increased the spacing between adjacent pulses to $T_r = 3T_p$. By comparison with Fig. 5, we note that the larger pulse spacing leaves more time to the pump to refill, so that the next pulse enjoys a larger pump and thus a larger gain, and thus it depletes the pump faster, with an ensuing increased power sag.

We next investigated the behavior of the same Raman amplifier when channel add-drop operations are performed. The amplifier now had $N = 8$ equally spaced input signals (channel spacing $\Delta\lambda = 0.8$ nm) from $\lambda_1 = 1552.4$ to $\lambda_8 = 1557.9$, with input power -2 dBm/ch, as in [4]. Figure 7 shows the output power excursion for the surviving channel $\lambda = 1552.4$ when adding/dropping 7 out of the 8 channels, for pump power $P_0 = 200$ mW and $P_0 = 400$ mW. We note the increased asymmetry between add and drop transients for the larger pump value, because of the larger saturation that follows the add operation. The drop transients are similar to those observed in Fig. 1.

4. Steady-state equation

The value of the steady-state depletion $x^{\rm ss}$ when CW signals are applied to the amplifier can be obtained from the dynamical equation (16) by using time invariant output powers $S_j^{\rm out}(x^{\rm ss})$,

$$x^{\rm ss} = \sum_{j=1}^{N} S_j^{\rm out}(x^{\rm ss}) w_j, \tag{22}$$

where we defined the weights $w_j \stackrel{\triangle}{=} \int_{-\infty}^{\infty} h_j(t)\,dt$. If we use the *exponential approximation* (A.3) and approximate $\chi \cong 1$, we get $w_j = h_{j0} d/\alpha_p \cong \lambda_j/(\lambda_p P_0)$, so that

$$x^{\rm ss} \cong \frac{\lambda_s}{\lambda_p} \frac{\sum_{j=1}^{N} S_j^{\rm out}(x^{\rm ss})}{P_0}, \tag{23}$$

an expression valid when the signals are closely spaced, at an average wavelength λ_s. This relation shows that *the depletion is approximately proportional to the ratio of total output signal power to the pump power*.

In (22) the dependence on $x^{\rm ss}$ can be made explicit,

$$x^{\rm ss} = \sum_{j=1}^{N} w_j S_j^{\rm in} e^{\{-\alpha_j L + g_j(1-x^{\rm ss})\}}, \tag{24}$$

and such transcendental equation is similar to Saleh's equation for the steady-state inversion in EDFAs [4]. Such equation should also be compared to a similar equation for the depletion Γ at steady-state that the authors have obtained under the impulsive pump-depletion approximation [12],

$$\Gamma^{\rm ss} = \sum_{j=1}^{N} \hat{c}_{jp} K_j S_j^{\rm in} e^{\{-\alpha_j L + g_j e^{-\Gamma^{\rm ss}}\}}, \tag{25}$$

where for long amplifiers and large gain, i.e., $\alpha_p L \gg 1$ and $Q_j > 4{-}5$ (see Appendix A), one finds

$$K_j = \frac{1 - e^{-(\alpha_p Q_j - \alpha_j)L}}{\alpha_p Q_j - \alpha_j} \cong \frac{1}{\alpha_p Q_j}.$$

If also $\Gamma^{\rm ss}$ is sufficiently small, so that $e^{-\Gamma^{\rm ss}} \cong 1 - \Gamma^{\rm ss}$, the two equations (24) and (25) essentially coincide, i.e., $x^{\rm ss} = \Gamma^{\rm ss}$. That this is indeed *exactly* so, one can convince himself by recalling that in the impulsive-pump depletion model, $\Gamma^{\rm ss}$ was found to be essentially independent of z [12], hence relation (13) gives

$$x^{\rm ss} = \frac{\int_0^L \overline{P}(z)\Gamma^{\rm ss}\,dz}{\int_0^L \overline{P}(z)\,dz} = \Gamma^{\rm ss}. \tag{26}$$

However, (25) holds also for much deeper saturation, i.e., when the approximation $e^{-\Gamma^{\rm ss}} \cong 1 - \Gamma^{\rm ss}$ fails. We were forced to introduce approximation (5) in order to make the dynamic model tractable.

5. Time constants of transients

The time constants involved in the transients can be easily made explicit when using the single-pole exponential approximation of the filter (A.3). In such case, in fact, Eq. (16) can be reduced to an ordinary differential equation (ODE) as follows. Define

$$x_j(t) \triangleq S_j^{\text{out}}(t) \otimes h_j(t) \tag{27}$$

which is an ODE in the unknown $x_j(t)$,

$$\dot{x}_j(t) = -\frac{1}{\tau} x_j(t) + h_{j0} S_j^{\text{out}}(t), \tag{28}$$

where $\tau \triangleq d/\alpha_p$. Now from (16) writes as $x(t) = \sum_{j=1}^{N} x_j(t)$, and therefore

$$\dot{x}(t) = -\frac{1}{\tau} x(t) + \sum_{j=1}^{N} h_{j0} S_j^{\text{in}}(t) e^{\{-\alpha_j L + g_j[1-x(t)]\}}. \tag{29}$$

Such ODE is quite similar to the dynamical equation of the average inversion in doped fiber amplifiers [4]. The time constant $\tau \triangleq d/\alpha_p$ plays here the role of the fluorescence time in EDFAs. The only significant difference from EDFAs is that the pump power does not explicitly appear in the ODE, but is hidden in the coefficients h_{j0} and in the log-gains g_j. How to include pump modulation, or pump relative intensity noise, will be explained in Section 6.

To understand the effect of the approximations involved in the derivation of (29), we compared the "exact" solution of (16) and the "approximate" solution of (29) when a pulse of duration 1 ms enters a transparent (i.e., of unit overall gain) distributed Raman amplifier whose transmission fiber is a non-zero dispersion shifted fiber (Raman gain coefficient $c_{jp} = 0.7$ [$\text{W}^{-1}\,\text{km}^{-1}$]) of increasing length. The relative pump depletion is shown in Fig. 8, with the exact solution in solid line, and the approximate solution in dashed line. We clearly note that the exponential approximation of the filter eliminates the ringing from the step response. Such ringing, however, is smaller and smaller as the amplifier length increases and the exponential approximation becomes closer to the actual filter response.

Having observed the similarity of (29) with the ODE governing transients in EDFAs, we next perform a linearization of the ODE (29) as is done in [3] for EDFAs, to find the response to N step input WDM signals and its time constant.

We start by writing the input signals and the state variable as a CW average value plus a deviation with respect to the CW:

$$\begin{aligned} S_j^{\text{in}}(t) &= S_j^{\text{ss}} + \Delta S_j(t), \\ x(t) &= x^{\text{ss}} + \Delta x(t). \end{aligned} \tag{30}$$

With such definitions, the dynamic gain is thus from (10)

$$G_j(t) = G_j^{\text{ss}} e^{-g_j \Delta x(t)} \cong G_j^{\text{ss}}\big(1 - g_j \Delta x(t)\big), \tag{31}$$

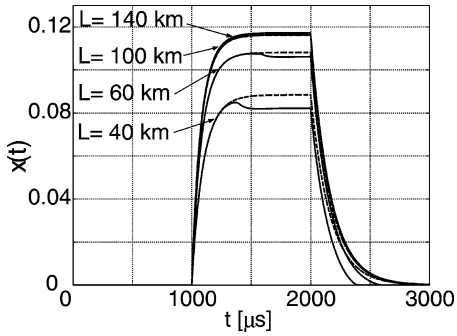

Fig. 8. Relative pump depletion for a distributed Raman amplifier based on a non-zero dispersion shifted fiber of increasing length L at transparency, when the input signal is a gate of duration 1 ms. Solid: solution of (16). Dashed: solution of (29).

being $G_j^{\rm ss}$ the steady state signal gain, and the approximation being accurate to within 5% when $g_j \Delta x(t) < 0.3$. Substitution of (30) and (31) in (29) leads to

$$\Delta\dot{x} = -\frac{x^{\rm ss}}{\tau} - \frac{\Delta x}{\tau} + \sum_{j=1}^{N} h_{j0}\big(S_j^{\rm ss} + \Delta S_j\big)\big(G_j^{\rm ss} - G_j^{\rm ss} g_j \Delta x\big) \tag{32}$$

which after subtraction of the steady state value obtained through (29) with $\dot{x} = 0$ simplifies to

$$\Delta\dot{x} = -\frac{\Delta x}{\tau} - \sum_{j=1}^{N} h_{j0} S_j^{\rm ss} G_j^{\rm ss} g_j \Delta x + \sum_{j=1}^{N} h_{j0} G_j^{\rm ss} \Delta S_j,$$

where we dropped the small term proportional to $\Delta S_j \Delta x$. Thus we finally get

$$\Delta\dot{x}(t) = -\frac{\Delta x(t)}{\tau_{\rm eff}} + \sum_{j=1}^{N} h_{j0} G_j^{\rm ss} \Delta S_j(t)$$

which corresponds to a first-order low-pass filtering of $\Delta S_j(t)$ with time constant

$$\tau_{\rm eff} \cong \frac{d/\alpha_p}{1 + \sum_{j=1}^{N} \frac{\hat{c}_{jp}}{\alpha_p} S_j^{\rm ss} G_j^{\rm ss}(L)} \cong \frac{d/\alpha_p}{1 + \frac{\sum_{j=1}^{N} S_j^{\rm out}(x^{\rm ss})}{S_s^{\rm is}}}, \tag{33}$$

where $S_j^{\rm ss}$ is the steady-state input power of the jth signal before the step discontinuity, and $G_j^{\rm ss}(L)$ is its saturated steady-state gain before the step, and we used (A.4) to approximate

$$h_{j0} g_j \cong \frac{\hat{c}_{jp}}{d Q_j} Q_j (1 - e^{-\alpha_p L}) \cong \frac{\hat{c}_{jp}}{d}.$$

The second approximation in (33) applies when the signals all have a similar gain, being λ_s their average wavelength and $S_s^{\rm is}$ their intrinsic saturation power (21). Thus, as seen in Fig. 9, power transients in saturated Raman amplifiers can be somewhat faster than the time constant d/α_p characterizing pump-induced relative intensity noise (cf. [13],

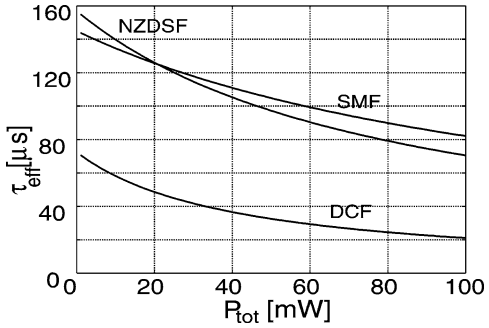

Fig. 9. Transient time constant (33) versus total output signal power $P_{\text{tot}} = \sum_i S_i^{\text{out}}(x^{\text{ss}})$ for counter-propagating pump, for various types of fiber (data as in Fig. 2).

see also next section) depending on the ratio of the total steady-state saturating power $P_{\text{tot}} = \sum_{j=1}^{N} S_j^{\text{out}}(x^{\text{ss}})$ to the intrinsic saturation power, a behavior very similar to that of saturated EDFAs [3,14].

6. Including pump intensity variations

It is possible to include pump relative intensity noise (RIN) or pump modulation in our analysis, and relate our results to those in [13]. Recall that in (3) we assumed a constant injected pump $P(t_p, L) = P_0$. Assume instead that $P(t_p, L) = P_0(1 - r(t_p))$, where $r(t)$ is a *small*[4] zero mean stochastic process. After linearization $e^{-\Gamma} \cong 1 - \Gamma$, the second equation in (3) becomes

$$P(t_p, z) = \overline{P}(z)\big(1 - r(t_p)\big)\big(1 - \Gamma(t_p, z)\big) \cong \overline{P}(z)\big(1 - r(t_p) - \Gamma(t_p, z)\big),$$

where we have dropped the negligible term $r(t_p)\Gamma(t_p, z)$. It is thus clear that the pump RIN term $r(t_p)$ is physically equivalent to the pump depletion term $\Gamma(t_p, z)$ as far as the signal dynamics are concerned. Following the same steps as in (3)–(11), we can thus define a RIN-induced pump depletion sensed by the signals as

$$x_r(t_s) = \frac{1}{L_p} \int_0^L e^{-\alpha_p(L - z')} r(t_s + dz')\, dz' \tag{34}$$

so that the output signal power is

$$S_j^{\text{out}}(t_s) = S_j^{\text{in}}(t_s) \exp\big\{-\alpha_j z + g_j\big(1 - x_\Gamma(t_s) - x_r(t_s)\big)\big\}, \tag{35}$$

[4] This model therefore does not apply to ON/OFF pump modulation, sometimes used in multi-pump amplifiers to reduce the pump-to-pump interactions [21].

where for clarity we have called x_Γ the depletion (12) caused by the signals. It is clear that the dynamical evolution of $x_r(t_s)$ is completely determined by the RIN process through (34), and if we make the change of variable $\tau = -dz'$ we get

$$x_r(t_s) = \frac{e^{-\alpha_p L}}{dL_p} \int_{-Ld}^{0} e^{-(\alpha_p/d)\tau} r(t_s - \tau)\, d\tau \tag{36}$$

which can be interpreted as a convolution operation [15], $x_r(t_s) = r(t_s) \otimes h^{\mathrm{RIN}}(t_s)$, where

$$h^{\mathrm{RIN}}(t) \triangleq \frac{1}{dL_p} e^{-(\alpha_p/d)(t+Ld)} \Pi\left(\frac{t + dL/2}{dL}\right) \tag{37}$$

is the impulse response of a non-causal filter, which is zero outside the interval $-Ld \leqslant t \leqslant 0$. We note in passing that such form of filtering due to the walk-off effect can be found also in other applications, such as for instance the study of cross-phase modulation, and a simple expression of its frequency response $H^{\mathrm{RIN}}(f)$ is known [16], with a 3 dB corner frequency $f_0 = \alpha_p/2\pi d = \alpha_p \upsilon/4\pi$ [13]. When the truncation due to the $\Pi(\cdot)$ function is absent, i.e., for long amplifiers $\alpha_p L \gg 1$, the above frequency response simplifies to an anticipating first-order low-pass filter,

$$h^{\mathrm{RIN}}(t) \triangleq h_0^{\mathrm{RIN}} e^{-(\alpha_p/d)(t+Ld)} U(t + Ld), \tag{38}$$

where $U(t)$ is the unit step function, and $h_0^{\mathrm{RIN}} = 1/dL_p$. The filter is non-causal, since the signal at retarded time t_s is affected by the future values of the pump RIN that have walked past the signal. As a numerical example, if we consider an SMF fiber with $\alpha_p = 0.28$ [dB/km] and group velocity $\upsilon_s = 2 \times 10^8$ [m/s], we get $f_0 \approx 1$ [kHz].

We can now define a total pump depletion state variable as

$$x(t_s) \triangleq x_\Gamma(t_s) + x_r(t_s)$$

which is the *superposition of the two perturbations*. Hence from (14) we have

$$\begin{aligned} x(t_s) &= x_r(t_s) + x_\Gamma(t_s) \\ &= x_r(t_s) + \frac{1}{L_p} \sum_{j=1}^{N} \hat{c}_{pj} \int_0^L e^{-\alpha_p(L-z_1)} \left\{ \int_{z_1}^{L} S_j^{\mathrm{in}}\big(t_s + d(z_1 - z_2)\big) \right. \\ &\qquad \left. \times G_j(z_2) \exp\big[-g_j(z_2) x\big(t_s + d(z_1 - z_2), z_2\big)\big]\, dz_2 \right\} dz_1, \end{aligned} \tag{39}$$

and with our usual simplification we get

$$x(t_s) \cong x_r(t_s) + \sum_{j=1}^{N} S_j^{\mathrm{in}}(t_s) e^{\{-\alpha_j z + g_j(1 - x(t_s))\}} \otimes h_j(t_s). \tag{40}$$

Using (40) and (35), we can thus give the block diagram shown in Fig. 10 of the Raman amplifier as a transformation of the signals. Such diagram could for instance be

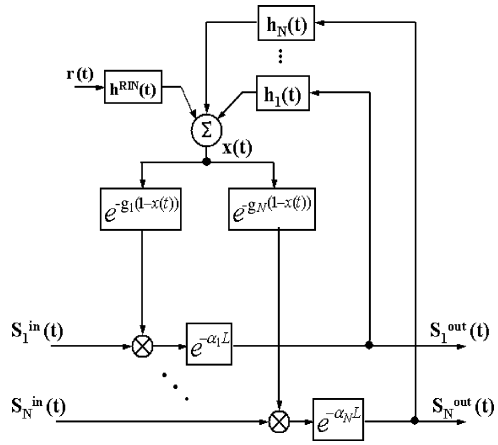

Fig. 10. Block diagram of the Raman amplifier, as a transformation of the input signals.

straightforwardly implemented in a commercial block-diagram simulator, such as Matlab Simulink^{TM} [7].

When the walk-off time dL is large, the gating function $\Pi(\cdot)$ does not affect the filters impulse response and one can use the exponential approximations (A.3) and (38), so that from (27) and (40) we have

$$x(t_s) = x_r(t_s) + \sum_j x_j(t_s),$$

and by taking time derivatives and using (28) and its counterpart for RIN,[5]

$$\dot{x}_r(t) = -\frac{1}{\tau} x_r(t) + h_0^{\mathrm{RIN}} r(t + Ld), \tag{41}$$

one finally gets the complete ODE that includes pump RIN:

$$\dot{x}(t_s) = -\frac{1}{\tau} x(t_s) + \sum_{j=1}^{N} h_{j0} S_j^{\mathrm{in}}(t_s) e^{\{-\alpha_j L + g_j[1-x(t_s)]\}} + h_0^{\mathrm{RIN}} r(t_s + Ld).$$

[5] Such relation is obtained from the Laplace transform of the RIN filter (38),

$$H(s) = h_0^{\mathrm{RIN}} e^{sLd}/(s + 1/\tau),$$

with $\tau = d/\alpha_p$, so that

$$\left(s + \frac{1}{\tau}\right) X_r(s) = h_0^{\mathrm{RIN}} R(s) e^{sLd},$$

where $R(s)$ is the Laplace transform of $r(t)$. We thus get

$$sX_r(s) = -\frac{X_r(s)}{\tau} + h_0^{\mathrm{RIN}} R(s) e^{sLd},$$

and taking inverse Laplace transforms one gets (41).

7. The multiple pump case

It is possible to extend the single state-variable model to the case where multiple counter-propagating pumps are present. The key idea is to first calculate the "bias point" of the extended model by computing the exact evolution of the pump powers along z in the absence of signals (we call these the *unsaturated* pump profiles), taking into account pump–pump interactions, and then use such information to keep track of the dynamic signal-induced depletion of each pump by means of one state variable for each pump.

Suppose we have M counter-propagating pumps, all propagating backwards at speed υ, and N WDM signals propagating forward at speed υ. The formal solution to the propagation equations in the retarded frames in this case becomes, for $p = 1, \ldots, M$ and $j = 1, \ldots, N$,

$$\begin{cases} P_p(t_p, z) = P_{0p} \exp\big(-\alpha_p(L-z) + \sum_{n=1}^{M} c_{pn} \int_z^L P_n(t_p, z')\, dz' \\ \qquad\qquad - \Gamma_p(t_p, z)\big), \\ S_j(t_s, z) = S_j^{\text{in}}(t_s) \exp\big(-\alpha_j z + \sum_{p=1}^{M} c_{jp} \int_0^z P_p(t_s + dz', z')\, dz'\big), \end{cases} \tag{42}$$

where again we have neglected the direct signal–signal Raman crosstalk, and $P_{0p} \triangleq P_p(t_p, L)$ is the constant injected power of the pth pump, and again we defined the pump depletion factors as

$$\Gamma_p(t_p, z) \triangleq \sum_{j=1}^{N} \hat{c}_{jp} \int_z^L S_j(t_p - dz', z')\, dz' \tag{43}$$

for $p = 1, \ldots, M$. Again we linearize $e^{-\Gamma_p} \cong 1 - \Gamma_p$, and the integral term in the signal equation in (42) becomes

$$c_{jp} \int_0^z P_p(t_s + dz', z')\, dz' = g_{jp}(z)\big(1 - x_p(t_s, z)\big),$$

where

$$\overline{P}_p(z) = P_{0p} \exp\left(-\alpha_p(L-z) + \sum_{n=1}^{M} c_{pn} \int_z^L \overline{P}_n(z')\, dz'\right) \triangleq P_{0p} \overline{f}_p(z)$$

is the (known) *unsaturated* z-profile of the pth pump with *shape factor* $\overline{f}_p(z)$, and we defined

$$\begin{cases} g_{jp}(z) \triangleq c_{jp} \int_0^z \overline{P}_p(z')\, dz', \\ x_p(t_s, z) \triangleq \frac{\int_0^z \overline{f}_p(z') \Gamma_p(t_s + dz', z')\, dz'}{\int_0^z \overline{f}_p(z')\, dz'}. \end{cases} \tag{44}$$

Now, as in (10), the signal power can be written as

$$S_j(t_s,z) = S_j^{\text{in}}(t_s)G_j(z)\exp\left\{-\sum_{p=1}^{M} g_{jp}(z)x_p(t_s,z)\right\}, \tag{45}$$

where the *unsaturated* steady-state gain is

$$G_j(z) = e^{-\alpha_j z+\sum_{p=1}^{M} g_{jp}(z)}. \tag{46}$$

Substitution of (43), (45) in the definition (44) gives for the state variables $x_p(t_s,L) \triangleq x_p(t_s)$,

$$\begin{aligned} x_p(t_s) = \frac{1}{L_p}\sum_{j=1}^{N}\hat{c}_{jp}\int_0^L \overline{f}_p(z_1)\Bigg\{\int_{z_1}^{L} S_j^{\text{in}}\big(t_s+d(z_1-z_2)\big) \\ \times G_j(z_2)\exp\Bigg[-\sum_{n=1}^{M} g_{jn}(z_2)x_n\big(t_s+d(z_1-z_2),z_2\big)\Bigg]dz_2\Bigg\}dz_1, \end{aligned} \tag{47}$$

where for brevity we defined $L_p \triangleq \int_0^L \overline{f}_p(z')\,dz'$. Again such complex equation can be drastically simplified by using the terms $g_{jn}(L)x_n(t_s+d(z_1-z_2),L)$ instead of the exact terms $g_{jn}(z_2)x_n(t_s+d(z_1-z_2),z_2)$ in the above integral. After the usual change of variables, and after dividing and multiplying by the *unsaturated gain* $G_j(L)$ in (46), one gets

$$\begin{aligned} x_p(t_s) = \sum_{j=1}^{N}\int_0^{dL} S_j^{\text{in}}(t_s-\tau)\exp\Big[-\alpha_j L+\sum_{n=1}^{M} g_{jn}\big[1-x_n(t_s-\tau)\big]\Big] \\ \times\frac{\hat{c}_{jp}}{dL_pG_j(L)}\left(\int_0^{L-\tau/d}\overline{f}_p(z')G_j(z'+\tau/d)\,dz'\right)d\tau, \end{aligned}$$

where $g_{jn} \triangleq g_{jn}(L)$, and the integration is again recognized as a convolution operation. Hence, the state variables $x_p(t_s)$ approximately satisfy the following *system of implicit integral equations*

$$\begin{aligned} x_p(t_s) = \sum_{j=1}^{N}\left\{S_j^{\text{in}}(t_s)\exp\Big[-\alpha_j L+\sum_{n=1}^{M} g_{jn}\big[1-x_n(t_s)\big]\Big]\right\}\otimes h_{jp}(t_s), \\ p=1,\ldots,M, \end{aligned} \tag{48}$$

where the filters impulse responses are

$$h_{jp}(t) = \frac{\hat{c}_{jp}}{dL_pG_j(L)}\left[\int_0^{L-t/d}\overline{f}_p(z')G_j\left(z'+\frac{t}{d}\right)dz'\right]\Pi\left(\frac{t-dL/2}{dL}\right). \tag{49}$$

Note that such filters depend on the (possibly flattened) overall unsaturated gain G_j (46). Such filters can be numerically evaluated once the exact unsaturated pump power profiles

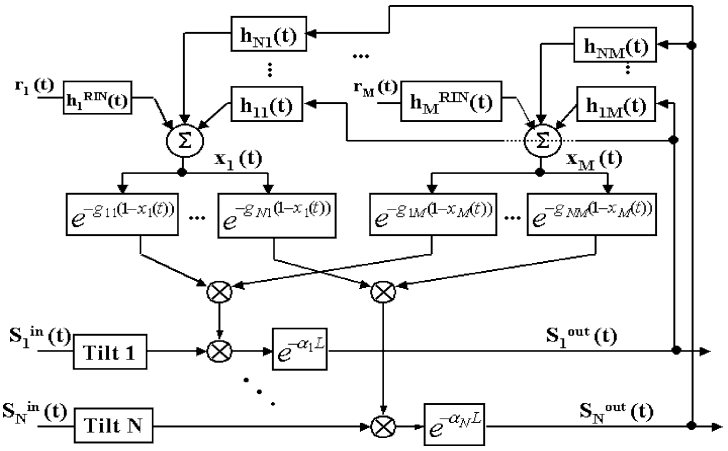

Fig. 11. Block diagram of Raman amplifier with M counter propagating pumps and N WDM input signals.

$\overline{f}_p(z)$ are known from the solution of the propagation equations for the pumps. Although it may be possible to introduce further simplifying assumptions to approximate the pump profiles $\overline{f}_p(z)$ [10,18], still a closed form for the filters does not seem readily obtainable, given the complicated form of the integrals in (49).

It is interesting to note that our model can be described by the input-output block diagram shown in Fig. 11, and can thus be implemented in commercially available block-diagram simulators [7]. In the scheme, we have also introduced further functional blocks: (i) the RIN filters $h_p^{\mathrm{RIN}}(t)$, $p = 1, \ldots, M$, Eq. (37), which take into account the (possibly present) relative intensity noise (RIN) or modulation on each pump; (ii) the pre-emphasis gain blocks Tilt_j, $j = 1, \ldots, N$, which are used as a simple approximate way to account for the power tilt in the signals' bandwidth due to direct signal-to-signal Raman crosstalk, which can be significant in distributed Raman amplifiers and takes place at the input, before amplification, as already discussed at the end of Section 2. Such method has already been successfully applied to saturated Raman amplifiers at steady state in [12].

In summary, using M pumps leads to M state variables $x_p(t_s)$, $p = 1, \ldots, M$, whose time evolution is found by iteratively solving the system (48). The procedure to solve the gain transient problem is the following:

1. Compute the pump evolution along z, $\overline{P}_p(z)$ in the absence of signals. This implies solving the steady-state propagation equation for pumps only, accounting for pump–pump power transfer;
2. Compute and store the MN filter responses, as per (49);
3. Iteratively solve the implicit system of update equations for pump depletions (48).

In essence, the procedure amounts to calculating the steady-state amplifier *bias point* without saturating signals (points 1 and 2), and then evaluating the time-varying signal-induced pump depletions from such bias point.

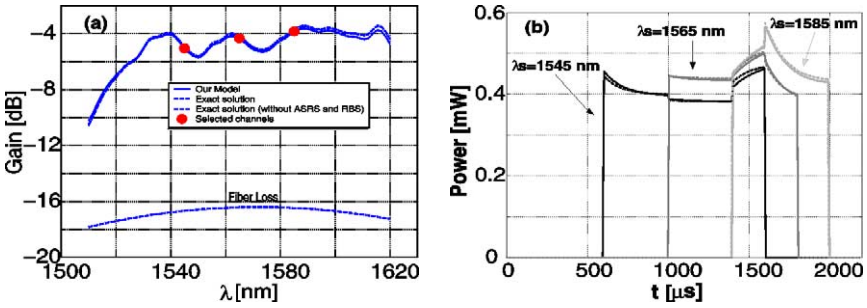

Fig. 12. Distributed multi-pumped Raman amplification in a 80 km NZDSF: (a) Raman saturated steady-state gain and fiber loss profile, and (b) output power time evolution of channels at 1545, 1565, 1585 nm.

The steady-state values of the state variables when the signals are CW are easily found as

$$x_p^{\mathrm{ss}} = \sum_{j=1}^{N} \left\{ S_j^{\mathrm{in}} e^{[-\alpha_j L + \sum_{n=1}^{M} g_{jn}[1-x_n^{\mathrm{ss}}]]} \right\} H_{jp}(0), \quad p = 1, \ldots, M,$$

and clearly depend on the value at $\omega = 0$ of the filters $H_{jp}(\omega)$. Once such equations are solved, the signal-saturated steady-state gain profile (45) is obtained.

It should be clear from the derivation that the main limit of such extended model is that it makes a distinction between a group of slightly perturbed pumps and a group of (possibly strongly) modulated signals. For instance, in resonant pumping, the pump closest to the signals behaves itself as a signal for the pumps at lower frequencies, and we should expect some discrepancy between model and simulation in such case.

To test the range of applicability of our extended model, we investigated several multi-pump schemes proposed in the literature, two of which will be presented in the next section.

7.1. Numerical verifications

We applied our model to two recently proposed Raman amplifiers, to test their dynamic behavior in deep saturation in order to get a realistic idea of the accuracy of our method. In this subsection we present the obtained results.

(A) We first consider the distributed amplifier presented in [19], which has an 80 km non-zero dispersion shifted fiber (NZDSF) with back-propagating pumps at 1423, 1443, 1464 and 1465 nm, with total input power of 590 mW. We consider the amplification of 80 WDM signals in the [1520, 1610] nm band, with 0 dBm/ch input power, which drive the amplifier in deep saturation.

In Fig. 12(a) we show the steady-state gain versus wavelength. The solid line shows the prediction of our model, the dashed line the exact solution of the complete propagation equations, and the dotted line—almost completely superposed to the previous one—the solution of the propagation equations when ASRS and DRB are switched off. The fiber loss profile across the channels is also shown in dash-dotted line. We note that in such heavily

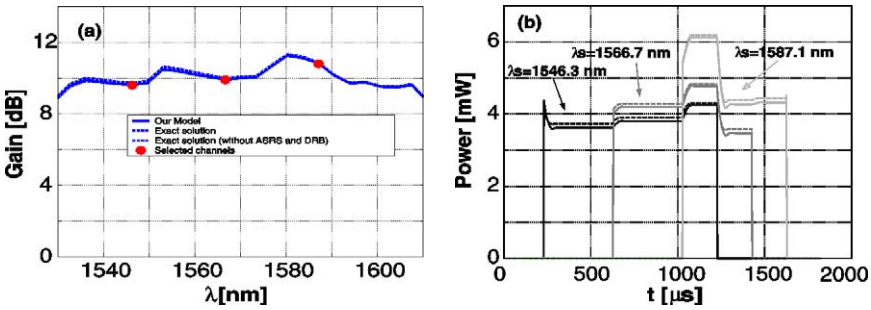

Fig. 13. Discrete multi-pumped Raman amplification in a DCF with length 5.5 km: (a) Raman saturated steady-state gain, and (b) output power time evolution of channels at 1546.3, 1566.7, 1587.1 nm.

saturated amplifier, noise and DRB are negligible, and our model very well matches the exact solution, the error with respect to the complete solution being less than 0.2 dB across the whole bandwidth, and mostly due to the approximations in the Tilt blocks [12]. When compared to the unsaturated gain profile [19], one notes a general gain decrease, and a pronounced tilt due both to saturation and to the signal–signal direct Raman interaction. In [19] it was noted that it is possible to change the Raman pumps in order to counteract such direct Raman tilt.

We then ON/OFF modulated all 80 channels with a random pattern of 10 bits and a bit duration of $T = 200$ ms, thus emulating time slotted packet transmission. The time behavior of three selected channels, marked with big dots in Fig. 12(a), is shown in Fig. 12(b), where solid line curves are the output of our model, while dotted lines are the output of the complete time-dependent propagation model (which neglects ASRS and DRB). We note sharp transients across the packets, which indicate a markedly saturated dynamic regime. To give an idea of the execution time savings, running the computations in Matlab on an 800 MHz Pentium III, takes 2 min for our model to both compute the steady-state profile and the transient behavior, while it took over 2 h for the complete solution of the propagation equations.

(B) We next consider the discrete Raman amplifier presented in [20], which has a 5 km dispersion compensating fiber (DCF) with 6 back-propagating pumps at 1428, 1445, 1467, 1484, 1491 and 1507 nm, with total injected power equal to 968 mW. We consider 24 input WDM signals in the range [1530, 1610] nm, with 4.5 dBm/ch input power, as in [20].

Figure 13(a) again shows the steady-state gain, and we note a better match between model and exact solution as compared with the distributed amplifier, because of the absence of direct Raman tilt. We then applied random ON/OFF modulation to all 24 channels with the same slot time of 200 ms, and the time behavior of the 3 selected channels marked in Fig. 13(a) is shown in Fig. 13(b). From the figure, it is clear that the amplifier is deeply saturated, and the match of our model with the exact solution is quite satisfactory, with the largest dynamical error being smaller than a few percent, and occurring at steady-state.

As for the computation times, our model took around 1 min to run both the static and dynamic simulation, while the exact static and dynamic solutions took about 15 min. Such

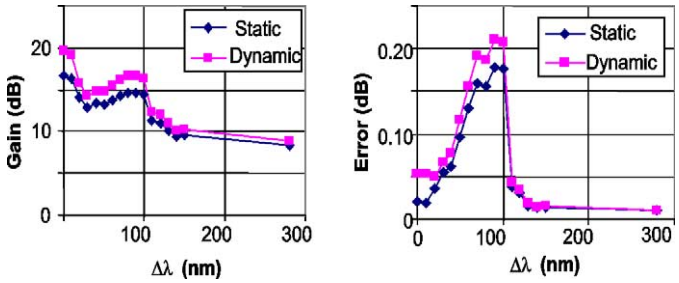

Fig. 14. Test of model accuracy with resonant pumping. (Left) Static and dynamic gain versus pump distance. (Right) Static and dynamic error between model and exact solution versus pump distance.

shorter time, obtained by keeping the same time resolution as that of the example (A), is due the fact that the amplifier is shorter, and the number of channels is smaller. Please note that the savings of our analytical model become more evident when the channel count is larger.

The multi-pump model has one extra limit with respect to the single pump model. Since the model makes a fundamental distinction between pumps and signals, it becomes less accurate in those cases in which the distinction is blurred, such as in resonant pumping.

To test such case, we tried a simple experiment. We launched a single channel at 1580 nm, consisting of a single 400-μs-long rectangular pulse of 1 mW input power, into a 10 km fiber with peak Raman gain coefficient 3.2 $W^{-1}\,km^{-1}$. We used two counter-propagating pumps: the first had 240 mW input power and was fixed at 1480 nm, i.e., at peak signal gain. The other had 180 mW input power. We recorded in Fig. 14 (left) both the static and the dynamic gain as the second pump was moved to lower wavelengths than 1480 nm. The static gain is the one experienced by the portion of the pulse that has reached steady-state, while the dynamic gain is the largest one in the transient, in practice coinciding with the unsaturated gain experienced by the leading edge of the pulse. In the figure, we note the initial decrease of the gain because the second pump provides less gain to the signal, followed by a subsequent increase of the gain because the second pump starts to amplify the first pump at 1480 nm by resonant pumping. In Fig. 14 (right) we also recorded both the static and the dynamic error, i.e., the largest and the steady-state error between the model and the exact solution of the propagation equations. The relative pump depletions for both pumps remained below 0.135. We note that the error is largest at 100 nm pump spacing, i.e., at resonant pumping, and can be more than 4 times larger than with normal pumping, although it remains below 0.2 dB in this example.

8. Co-propagating pump

Let us now consider the case of co-propagating pump. We will closely follow the derivations for the counter-propagating pump. In this case both pump and signals are injected at $z_i = 0$ and propagate at group velocity υ_p and υ_s in the positive z direction, with walk-off

$d \cong D(\lambda_s - \lambda_p)$ dictated by the GVD parameter D.[6] Neglecting direct signal crosstalk, the solution at coordinate $z_0 = z \leqslant L$ of the propagation equations for the co-propagating pump configuration in the retarded frames is obtained from (2) as

$$\begin{cases} S_j(t_s, z) = S_j^{\text{in}}(t_s) \exp\{-\alpha_j z + c_{jp} \int_0^z P(t_s + dz', z')\, dz'\}, \\ P(t_p, z) = P_0 e^{-\alpha_p z} e^{-\Gamma(t_p, z)}, \end{cases} \tag{50}$$

where again we defined

$$\Gamma(t_p, z) \triangleq \sum_{j=1}^{N} \hat{c}_{jp} \int_0^z S_j(t_p - dz', z')\, dz'. \tag{51}$$

By closely following the derivation for the counter-propagating pump, one defines the unsaturated log-gain as $g_j(z) \triangleq (1 - e^{-\alpha_p z}) c_{jp} P_0/\alpha_p$, so that the unsaturated gain $G_j(z)$ is still given by (9), and the pump relative depletion as

$$x(t_s) = \frac{1}{L_p} \int_0^L e^{-\alpha_p z} \Gamma(t_s + dz, z)\, dz. \tag{52}$$

With standard manipulations, one arrives at the following update equation for the pump depletion:

$$x(t_s) = \frac{1}{L_p} \sum_{j=1}^{N} \hat{c}_{jp} \int_0^L e^{-\alpha_p z_1} \left\{ \int_0^{z_1} S_j^{\text{in}}\big(t_s + d(z_1 - z_2)\big) \times G_j(z_2) \exp\big[-g_j(z_2) x\big(t_s + d(z_1 - z_2), z_2\big)\big]\, dz_2 \right\} dz_1. \tag{53}$$

We may try here the same trick as in the counter-propagating pump case, namely using $\exp[-g_j x(t_s + d(z_1 - z_2), L)]$ instead of the correct term $\exp[-g_j(z_2) x(t_s + d(z_1 - z_2), z_2)]$ in the above integral. Such approximation make sense for co-pumped amplifiers whose length L corresponds to maximum signal gain. With such assumption, one gets again the update equation (16) for the depletion, where $S_j^{\text{out}}(t_s, x(t_s))$ is given again in (11), but now h_j is the impulse response of the following linear filter:

$$h_j(t) = \frac{\hat{c}_{jp}}{dL_p G_j(L)} \left[\int_{-t/d}^{L} e^{-\alpha_p z'} G_j\left(z' + \frac{t}{d}\right) dz' \right] \Pi\left(\frac{t + dL/2}{dL}\right). \tag{54}$$

As we see, the filter is non-causal (i.e., it extends to negative time) when $d > 0$, i.e., when the pump is faster than the signals, since the depleted pump reaches past sections of a packet and distorts them with echoes of the future. Appendix A provides a closed form expression of the above filter.

[6] Such approximation is valid when pump and signals are either both to the left or both to the right of the zero dispersion wavelength λ_0, as in SMF and NZDSF$^-$ fibers. The above does not hold for NZDSF$^+$ fibers, where λ_0 is to the left of the C-band, but to the right of the pump wavelength.

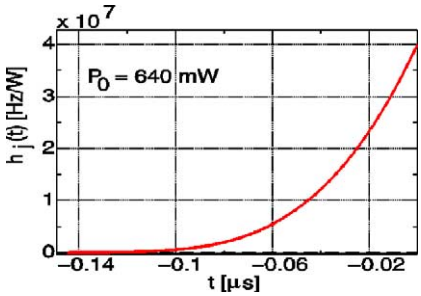

Fig. 15. Filter impulse response $h_j(t)$ (A.5) for co-propagating pump, in the case in which the pump is faster than the signal.

8.1. Numerical verifications

In the following, we present a somewhat artificial example in which the fiber parameters of the Raman amplifier are those of the DCF used in the calculations in Fig. 1, but the dispersion is $D = +110$ ps/nm/km and thus the pump is faster than the signal, in order to highlight the effect of an anti-causal $h_j(t)$ filter.

Figure 15 shows $h_j(t)$ in (54), numerically evaluated as per (A.5) in Appendix A, for an $L = 14$ km amplifier made of fiber with Raman coefficient $c_{jp} = 2$ [W^{-1} km^{-1}], with signal wavelength $\lambda_j = 1545.3$ nm and pump wavelength $\lambda_p = 1454.7$ nm, with a co-propagating pump $P_0 = 640$ mW. The filter is zero beyond $t < -dL = -D\Delta\lambda L = -0.15$ μs.

We next made the following experiment. The same amplifier was first counter-pumped, and then co-pumped with the same pump power to check similarities and differences between the two schemes. The input signal in the counter-pumped scheme is the same two-pulse (1 mW pulse followed by a 0.1 mW pulse) single-channel sequence used in Fig. 1, with duration 400 μs per pulse. Each pulse was long enough to observe the complete saturation transient on it, as in Fig. 1. The time waveforms of the output pulses are shown in Fig. 16, left column. We are already familiar with the large spike on the leading edge of the first pulse.

We then used the inverted sequence (0.1 mW pulse followed by 1 mW pulse) to feed the co-pumped amplifier, but now the pulses had a much shorter duration of 0.2 μs, long enough to observe the complete saturation transient on them. The output pulses are shown in Fig. 16, right column. We note here that the power spike is on the trailing edge of the pulse, an effect due to the fact that the pump overtakes the signal, and is thus connected to the non-causality of the filter $h_j(t)$. In the insets, we also show the time behavior of the pump depletion $x(t)$. The top row figures were obtained for the same injected pump power $P_0 = 640$ mW, while the bottom row figures used $P_0 = 400$ mW. It is known that in the unsaturated regime co- and counter-pumping with the same power produce the same unsaturated gain. This is visible in the figures, since the leading edge of the pulse in the counter-pumped scheme and the lagging edge of the pulse in the co-pumped scheme experience such unsaturated gain, and thus have the same power level.

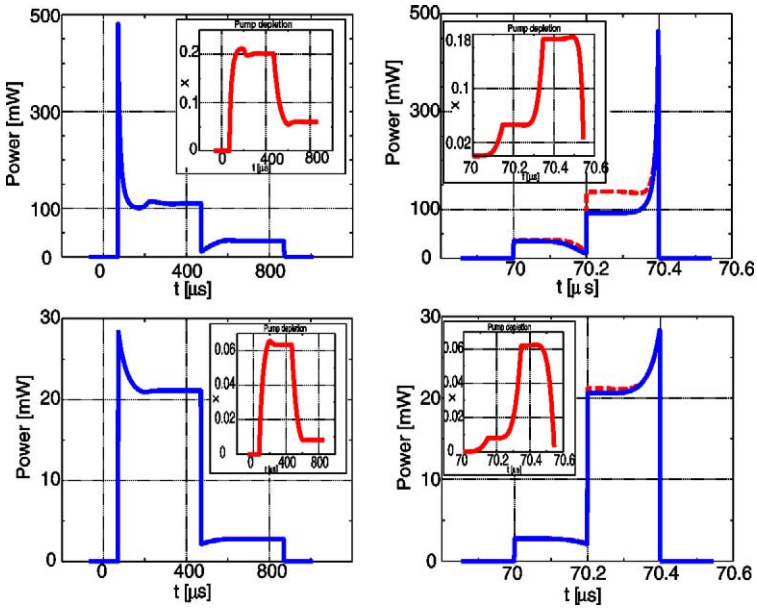

Fig. 16. Power out of a 14 km amplifier for the case of counter-pumping (left column) and co-pumping (right column), for injected power $P_0 = 640$ mW (top row), and $P_0 = 400$ mW (bottom row). Relative pump change $x(t)$ shown in the insets. Solid lines: exact solution (1); dashed lines: model (16).

Solid lines represent the exact solution of the propagation equations (1). By comparison between left and right columns, we note that the amount of saturation, and thus power sag on the pulses, is about the same in the two schemes.

Dashed lines represent the solution of the model (16). Such lines are coinciding with the exact solution in both cases of counter-pumping (left column) and are thus hidden by the solid line curves, since the depletion $x(t)$ is well below 30% in both cases.

On the contrary, we note that the model for co-pumping is much less precise, with an error on the steady-state level that increases with increased pumping. We note from the figure that the reproduction of the transient is acceptable, with error below 5%, when the depletion $x(t)$ remains below 6%.

In any case, we note that the model is able to correctly reproduce the time constants of the transients in both cases.

Note that the major problem in the experimental observation of power transients in the co-pumped scheme is connected to the very short transient times, of the order of tens of nanoseconds, and that the switch-on and switch-off times of the pulses must be in the nanosecond time scale order to reproduce the same transients we obtained in the simulation. If one uses an optical modulator with switching time comparable to those of the transients, one gets a much smoother time profile of the output pulse.

Finally, we note from the exponential approximation (A.6) of the filter $h_j(t)$ that the fast transient times in the co-pumped case are a consequence of the well-known difference of the RIN filter bandwidth in the co- and counter-propagating configurations [13,15].

9. Conclusions

We presented a comprehensive analytical treatment of transient gain dynamics in saturated Raman amplifiers. Although the exact solution of the propagation equations is always simple to compute using standard numerical integration of the propagation partial differential equations, such solutions require very long computation times, especially in large WDM systems, and the numerical integration does not provide any insight into the nature of the solutions and the quantitative importance of the various system parameters.

The modeling presented in this paper starts in fact from the propagation equations, and by introducing sensible approximations reduces the extremely complex differential equations to familiar forms in system and control theory, namely, block diagrams which can be readily implemented using commercially available block diagram simulators.

The true value of such system model is twofold.

First, transient simulation times are almost independent of the number of WDM channels, as long as the level of saturation falls within the range of applicability of the model. Therefore, enormous simulation time savings are possible for very large WDM systems, such as those envisaged both for the next generation metropolitan area networks, and for the all optical wide area networks. Solutions such as Internet protocol (IP) over WDM packet networks are examples in which our models shall provide the only possibility of following the complex dynamics of the interconnected network of Raman and erbium doped fiber amplifiers, thanks to the availability of simple block diagrams for both of them.

Second, block diagram models naturally lead to simple approximate expressions of the main system parameters of interest. In this paper, for instance, we have derived closed form expressions for the power sag across pulses and for the transient time constants versus amplifier output power. The key amplifier parameters that shape the transients have been identified and quantified.

The extension of the counter-propagating pump model to the multiple pump case increases the applicability of the model to very practical wide-band amplifiers.

We have also proven that the co-propagating case can be partially tackled using the same tools, although the accuracy is much less than that of the counter-propagating pump case.

It may be conjectured that a mixed pumping scheme in which a small fraction of the gain comes from co-pumping and the rest from counter-pumping could also be tackled, although this remains an open question for future investigations.

Let us now move to the possible countermeasures against such transients. A natural question to ask is the following: given that we have spotted a single state variable, like in the EDFA, and that the update equations for such state variable are similar to those in the EDFA, is it possible to gain-clamp the counter-pumped Raman amplifier? Classical gain clamping in EDFAs consists of feeding the output signal at a specific wavelength λ_l back to the input so that a standing wave exists at that frequency that saturates the inversion (i.e., the state variable) and clamps it [14]. The effectiveness of such feedback control relies on the fact that the feedback delay is much smaller than the time scale of the transients inside the system.

In the Raman amplifier, a perturbation of the standing wave operated by an incoming packet at λ_s creates a “notch” in the pump power that propagates backwards to the input.

The reaction time of the standing wave is at least the propagation time inside the amplifier. Hence, by the time the standing wave reacts to the signal power variation, the notch has propagated to the input, and thus we have an undampened power sag across the signal output pulse.

In other terms: since the delay between the stimulus and the start of the control action is of the same order as the time scale of the transients, then any feedback control system is ineffective to dampen the transients. From the experimental results in [22] one can note that gain-clamping a discrete Raman amplifier can in fact eliminate the large overshoot on the leading edge of the pulse, caused by the unsaturated gain enjoyed by the pulse front, because the standing laser light keeps the gain at deep saturation. However, from the same results (Fig. 6 in that reference) one observes that the subsequent oscillations are not dampened by the clamping laser, because of the control delay reason we mentioned above.

So, how can we counteract such transients? The simplest countermeasure is the adoption of a hybrid dual-stage Raman–EDFA configuration, in which the first Raman stage does not reach output signal powers large enough to deeply saturate it, and the following EDFA stage can then be gain clamped. Another option is to control the pump current with a control signal that is aware of the entering pulses. The analytical framework proposed in this paper should make it possible to extend previous analytical investigations on gain clamping [14] to the Raman amplifier as well.

Appendix A. Filters and their approximation

In this Appendix we provide closed-form analytical expressions of the filter $h_j(t)$ in (17) and (54) as power series expansions, along with simple single-pole low-pass approximations, valid for long Raman amplifiers.

A.1. Counter-propagating pump

We first derive expressions for $h_j(t)$ in (17). Let us start by considering the following function:

$$F_j(y) = \frac{1}{G_j(L)} \int_0^{L-y} e^{-\alpha_p(L-z')} G_j(z'+y)\, dz'.$$

Using (9), with $Q_j \triangleq c_{jp} P_0/\alpha_p$ [11], we get for $0 \leqslant y \leqslant L$

$$F_j(y) = \frac{\exp\{-\alpha_p L - \alpha_j y - Q_j e^{-\alpha_p L}\}}{\exp\{-\alpha_j L + Q_j(1-e^{-\alpha_p L})\}} \times \int_0^{L-y} \exp\left\{(\alpha_p - \alpha_j)z' + Q_j e^{-\alpha_p(L-y)} e^{\alpha_p z'}\right\} dz'.$$

Performing the following change of variable $t = Q_j e^{-\alpha_p(L-y)} e^{\alpha_p z'}$, one gets

$$F_j(y) = \frac{e^{-\alpha_p L+\alpha_j(L-y)-Q_j}}{\alpha_p} Q_j^{(\alpha_j/\alpha_p-1)} \int_{Q_j \exp\{-\alpha_p(L-y)\}}^{Q_j} t^{-(\alpha_j/\alpha_p)} e^t \, dt$$

$$= \frac{e^{-Q_j}}{\alpha_p} e^{-\alpha_p y} Q_j^{(\alpha_j/\alpha_p-1)} \big[\Psi(Q_j, \alpha_j/\alpha_p) - \Psi\big(Q_j e^{-\alpha_p(L-y)}, \alpha_j/\alpha_p\big)\big],$$

where $\Psi(x,a)$ is defined as

$$\Psi(x,a) \stackrel{\triangle}{=} \int_0^x t^{-a} e^t \, dt, \quad 0 < a < 1,$$

and we have assumed $\alpha_p \neq \alpha_j$.[7] Such function can be quickly numerically evaluated by the following series

$$\Psi(x,a) = x^{1-a} \sum_{n=0}^{\infty} \frac{x^n}{(n+1-a)n!}$$

obtained by expanding the exponential in a Taylor series about $x = 0$ and then performing the integrations.

Therefore using the above results, one gets for the filter impulse response when $\alpha_p \neq \alpha_s$

$$h_j(t) = \frac{\hat{c}_{jp} e^{-Q_j}}{dL_p \alpha_p} Q_j^{(\alpha_j/\alpha_p-1)} e^{-(\alpha_p/d)t} \times \big[\Psi(Q_j, \alpha_j/\alpha_p) - \Psi\big(Q_j e^{-\alpha_p(L-t/d)}, \alpha_j/\alpha_p\big)\big] \Pi\left(\frac{t - dL/2}{dL}\right), \quad \text{(A.1)}$$

and when $\alpha_p = \alpha_j$

$$h_j(t) = \frac{\hat{c}_{jp} e^{-Q_j}}{dL_p \alpha_p} e^{-(\alpha_p/d)t} \big[\mathrm{Ei}(Q_j) - \mathrm{Ei}\big(Q_j e^{-\alpha_p(L-t/d)}\big)\big] \Pi\left(\frac{t - dL/2}{dL}\right). \quad \text{(A.2)}$$

For long amplifiers such as the distributed Raman amplifiers, in which $L \gg 1/\alpha_p$, the filter can be simplified to

$$h_j(t) \cong h_{j0} e^{-(\alpha_p/d)t}, \quad \text{(A.3)}$$

where

$$h_{j0} = \frac{\hat{c}_{jp}}{dQ_j} \chi,$$

$$\chi \stackrel{\triangle}{=} e^{-Q_j} Q_j^{\alpha_j/\alpha_p} \Psi(Q_j, \alpha_j/\alpha_p), \quad \text{(A.4)}$$

[7] If $\alpha_p = \alpha_j$, the function $\Psi(x,1)$ is not well defined, since the integral diverges at $t = 0$. However, in this case one can use the exponential integral function $\mathrm{Ei}(x) \stackrel{\triangle}{=} \int_{-\infty}^{x} z^{-1} e^z \, dz$, $z \in C$, and get

$$F_j(y) = \frac{e^{-Q_j}}{\alpha_p} e^{-\alpha_p y} \big[\mathrm{Ei}(Q_j) - \mathrm{Ei}(Q_j e^{-\alpha_p(L-y)})\big].$$

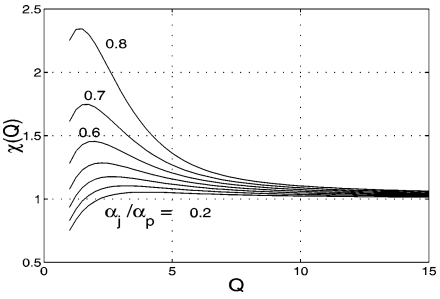

Fig. 17. Function χ defined in (A.4).

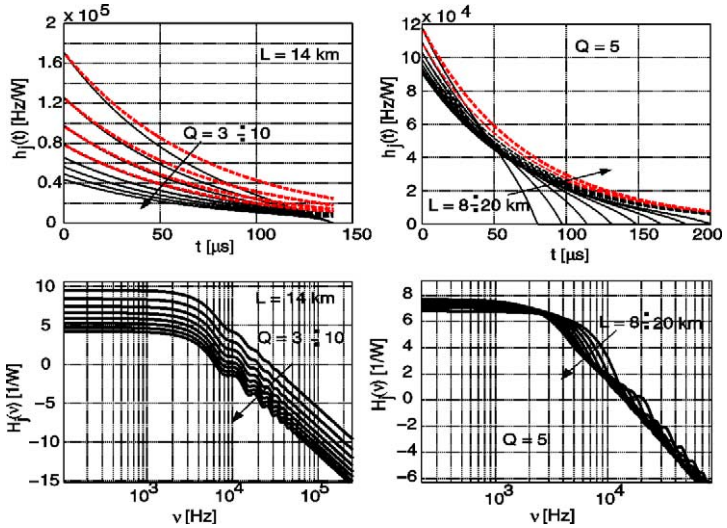

Fig. 18. Top row: filter impulse response $h_j(t)$ (solid line) and its exponential approximation (dashed line). Bottom row: its Fourier transform $H_j(\nu)$.

where the function χ is close to 1 except for a small interval of Q values where it swings up to 2 for $\alpha_j/\alpha_p < 0.8$, as shown in Fig. 17.

The top row in Fig. 18 shows $h_j(t)$, Eq. (A.1), in solid line, and its exponential approximation (A.3) in dashed line, for (left) a 14 km amplifier and increasing values of Q, and (right) for $Q = 5$ and increasing L. All filters are zero beyond $t = dL$, which is twice the propagation time inside the amplifier (we assumed $\upsilon_s = 2 \times 10^8$ m/s). In the calculations, we used $\alpha_j = 0.46$ dB/km, $\alpha_p = 0.6$ dB/km, $c_{jp} = 2$ [W^{-1} km^{-1}], corresponding to a dispersion compensating fiber (DCF) with signal wavelength $\lambda_j = 1545.3$ nm, and pump wavelength $\lambda_p = 1454.7$ nm [5]. The bottom row in Fig. 18 shows the corresponding filter frequency response $H_j(\nu)$. The frequency oscillations are due to the truncation operated by the $\Pi(\cdot)$ gating function, whose Fourier transform has a sine-like behavior with such oscillations. Note that all filters have a 3 dB breakpoint at a frequency close to that of the exponential approximation $\nu = \alpha_p/2\pi d$.

A.2. Co-propagating pump

In this section we will provide a closed-form analytical expression of the filter $h_j(t)$ in (54).

Let us start by considering the following function:

$$F_j(y) = \frac{1}{G_j(L)} \int_{-y}^{L} e^{-\alpha_p z'} G_j(z'+y)\, dz'.$$

Using (9), we get for $0 \leqslant y \leqslant L$

$$F_j(y) = \frac{\exp\{\alpha_j y + Q_j\}}{\exp\{-\alpha_j L + Q_j(1-e^{-\alpha_p L})\}} \int_{y}^{L} e^{-(\alpha_p+\alpha_j)z' - Q_j e^{-\alpha_p(z'-y)}}\, dz'.$$

Performing the change of variable $t = Q_j e^{-\alpha_p(z'-y)}$, one gets

$$F_j(y) = \frac{e^{\alpha_j L + Q_j e^{-\alpha_p L}}}{\alpha_p Q_j^{(1+\alpha_j/\alpha_p)}} \left[\gamma\left(Q_j, 1+\frac{\alpha_j}{\alpha_p}\right) - \gamma\left(Q_j e^{-\alpha_p(L-y)}, 1+\frac{\alpha_j}{\alpha_p}\right)\right] e^{-\alpha_p y},$$

where $\gamma(x,a)$ is the well-known incomplete gamma function,

$$\gamma(x,a) \stackrel{\triangle}{=} \int_0^x t^{a-1} e^{-t}\, dt, \quad a > 0,$$

where $a = 2$ when $\alpha_j = \alpha_p$. Such function can be quickly numerically evaluated by the following series

$$\gamma(x,a) = \sum_{n=0}^{\infty} \frac{(-1)^n x^{a+n}}{(n+a)n!}$$

obtained by expanding the exponential in a Taylor series about $x = 0$ and then performing the integrations. When a is an integer, then we can use the exact expression

$$\gamma(x,a) = (a-1)!\left[1 - e^{-x} \sum_{n=0}^{a-1} \frac{x^n}{n!}\right].$$

Therefore using the above results, one gets the filter impulse response as

$$h_j(t) = \frac{\hat{c}_{jp}}{dL_p} F\left(-\frac{t}{d}\right) \Pi\left(\frac{t+dL/2}{dL}\right)$$

and thus

$$\begin{aligned} h_j(t) = {} & \frac{\hat{c}_{jp}}{dL_p} \frac{e^{\alpha_j L + Q_j e^{-\alpha_p L}}}{\alpha_p Q_j^{(1+\alpha_j/\alpha_p)}} e^{(\alpha_p/d)t} \\ & \times \left[\gamma\left(Q_j, 1+\frac{\alpha_j}{\alpha_p}\right) - \gamma\left(Q_j e^{-\alpha_p(L+t/d)}, 1+\frac{\alpha_j}{\alpha_p}\right)\right] \Pi\left(\frac{t-dL/2}{dL}\right). \end{aligned} \tag{A.5}$$

For long amplifiers in which $L \gg 1/\alpha_p$, the filter can be simplified to

$$h_j(t) \cong h_{j0} e^{(\alpha_p/d)t}, \quad t \leqslant 0, \tag{A.6}$$

and zero elsewhere, being

$$\begin{aligned} h_{j0} &\cong \frac{\hat{c}_{jp}}{d} \frac{e^{\alpha_j L + Q_j e^{-\alpha_p L}}}{Q_j^{(1+\alpha_j/\alpha_p)}} \gamma\left(Q_j, 1 + \frac{\alpha_j}{\alpha_p}\right) \\ &\cong \frac{\hat{c}_{jp} e^{\alpha_j L}}{d} \frac{1 - e^{-Q_j}(1+Q_j)}{Q_j^2} \cong \frac{\hat{c}_{jp} e^{\alpha_j L}}{d Q_j^2}, \end{aligned} \tag{A.7}$$

where in the first line we dropped the second $\gamma(.)$ term; in second line we neglected $Q_j e^{-\alpha_p L}$ with respect to $\alpha_j L$, and approximated $a \cong 2$ and thus $\gamma(x, 2) = 1 - e^x(1+x)$; and in the third line we assumed $e^{Q_j} \ll 1$. Such exponential filter has the same time constant as the RIN filter for co-propagating pump [13].

References

[1] A.K. Srivastava, J.L. Zyskind, J.W. Sulhoff, EDFA transient response to channel loss in WDM transmission system, IEEE Photon. Technol. Lett. 9 (1997) 386–388.

[2] Y. Sun, J.L. Zyskind, A.K. Srivastava, Average inversion level, modeling, and physics of erbium-doped fiber amplifiers, J. Sel. Areas Quantum Electron. 3 (1997) 991–1007.

[3] Y. Sun, A.A.M. Saleh, J.L. Zyskind, D.L. Wilson, A.K. Srivastava, J.W. Sulhoff, Time dependent perturbation theory and tones in cascaded erbium-doped fiber amplifier systems, IEEE J. Lightwave Technol. 15 (1997) 1083–1087.

[4] A. Bononi, L.A. Rusch, Doped fiber amplifier dynamics: a system perspective, IEEE J. Lightwave Technol. 16 (1998) 945–956.

[5] C.-J. Chen, W.S. Wong, Transient effects in Raman optical amplifiers, in: Proc. OAA 2001, Stresa, Italy, July, 2001, paper OMC2.

[6] M. Karàsek, M. Menif, Channel addition/removal response in Raman fiber amplifiers: modeling and experimentation, IEEE J. Lightwave Technol. 20 (2002) 1680–1687.

[7] S. Novak, R. Gieske, Simulink model for EDFA dynamics applied to gain modulation, IEEE J. Lightwave Technol. 20 (2002) 986–992.

[8] Y. Sugaya, S. Muro, Y. Sato, E. Ishikawa, Suppression method of transient power response of Raman amplifier caused by channel add-drop, in: Proc. ECOC 2002, Vol. 2, Copenhagen, Denmark, September, 2002, paper 5.2.3.

[9] S. Tariq, J.C. Palais, A computer model of non-dispersion-limited stimulated Raman scattering in optical fiber multiple-channel communications, IEEE J. Lightwave Technol. 11 (1993) 1914–1924.

[10] D.N. Christoulides, R.B. Jander, Evolution of stimulated Raman crosstalk in wavelength division multiplexed systems, IEEE Photon. Technol. Lett. 8 (1996) 1722–1724.

[11] M.-S. Kao, J. Wu, Signal light amplification by stimulated Raman scattering in an N-channel WDM optical fiber communication system, IEEE J. Lightwave Technol. 7 (1989) 1290–1299.

[12] A. Bononi, M. Papararo, A. Vannucci, The impulsive pump depletion in saturated Raman amplifiers, IEE Electron. Lett. 37 (14) (2001) 886–887.

[13] C.R.S. Fludger, V. Handerek, R.J. Mears, Pump to signal RIN transfer in Raman fiber amplifiers, IEEE J. Lightwave Technol. 19 (2001) 1140–1148.

[14] A. Bononi, L. Barbieri, Design of gain-clamped doped-fiber amplifiers for optimal dynamic performance, IEEE J. Lightwave Technol. 17 (1999) 1229–1240.

[15] K.-P. Ho, Statistical properties of stimulated Raman crosstalk in WDM systems, IEEE J. Lightwave Technol. 18 (2000) 915–921.

[16] A. Bononi, C. Francia, G. Bellotti, Impulse response of cross-phase modulation filters in multi-span transmission systems with dispersion compensation, Opt. Fiber Technol. 4 (1998) 371–383.
[17] M. Mehendale, A. Kobyakov, M. Vasilyev, S. Tsuda, Stimulated Brillouin scattering in Raman-amplified dispersion compensating fibers, in: Proc. OFC 2002, Anaheim, CA, March, 2002, pp. 560–561.
[18] X. Zhou, C. Lu, P. Shum, T.H. Cheng, A simplified model and optimal design of a multiwavelength backward-pumped fiber Raman amplifier, IEEE Photon. Technol. Lett. 13 (2001) 945–947.
[19] C.R.S. Fludger, V. Handerek, Ultra-wide bandwidth Raman amplifiers, in: Proc. OFC 2002, Anaheim, CA, March, 2002, paper TuJ3, pp. 60–62.
[20] L. Grüner-Nielsen, Y. Qian, B. Pàlsdòttir, P.B. Gaarde, S. Dyrbøl, T. Veng, Module for simultaneous C + L band dispersion compensation and Raman amplification, in: Proc. OFC 2002, Anaheim, CA, March, 2002, paper TuJ6, pp. 65–66.
[21] L.F. Mollenauer, A.R. Grant, P.V. Mamyshev, Time-division multiplexing of pump wavelengths to achieve ultrabroadband, flat, backward-pumped Raman gain, IEEE Opt. Lett. 27 (2002) 592–594.
[22] S.S.-H. Yam, F.-T. An, E.S.-T. Hu, M.E. Marhic, T. Sakamoto, L.G. Kazovsky, Gain-clamped S-band discrete Raman amplifier, in: Proc. OFC 2002, Anaheim, CA, March, 2002, pp. 385–387.